EPR Investigation of Cu^{2+}-Substituted Photosynthetic Bacterial Reaction Centers: Evidence for Histidine Ligation at the Surface Metal Site

Lisa M. Utschig,* Oleg Poluektov, David M. Tiede, and Marion C. Thurnauer

Chemistry Division, Argonne National Laboratory, Argonne, Illinois 60439

Received August 3, 1999; Revised Manuscript Received November 17, 1999

ABSTRACT: The coordination environments of two distinct metal sites on the bacterial photosynthetic reaction center (RC) protein were probed with pulsed electron paramagnetic resonance (EPR) spectroscopy. For these studies, Cu^{2+} was bound specifically to a surface site on native Fe^{2+}-containing RCs from *Rhodobacter sphaeroides* R-26 and to the native non-heme Fe site in biochemically Fe-removed RCs. The cw and pulsed EPR results clearly indicate two spectroscopically different Cu^{2+} environments. In the dark, the RCs with Cu^{2+} bound to the surface site exhibit an axially symmetric EPR spectrum with $g_{||} = 2.24$, $A_{||} = 160$ G, $g_{\perp} = 2.06$, whereas the values $g_{||} = 2.31$, $A_{||} = 143$ G, and $g_{\perp} = 2.07$ were observed when Cu^{2+} was substituted in the Fe site. Examination of the light-induced spectral changes indicate that the surface Cu^{2+} is at least 23 Å removed from the primary donor (P^+) and reduced quinone acceptor (Q_A^-). Electron spin−echo envelope modulation (ESEEM) spectra of these Cu−RC proteins have been obtained and provide the first direct solution structural information about the ligands in the surface metal site. From these pulsed EPR experiments, modulations were observed that are consistent with multiple weakly hyperfine coupled ^{14}N nuclei in close proximity to Cu^{2+}, indicating that two or more histidines ligate the Cu^{2+} at the surface site. Thus, metal and EPR analyses confirm that we have developed reliable methods for stoichiometrically and specifically binding Cu^{2+} to a surface site that is distinct from the well characterized Fe site and support the view that Cu^{2+} is bound at or near the Zn site that modulates electron transfer between the quinones Q_A and Q_B ($Q_A^-Q_B \rightarrow Q_AQ_B^-$) (Utschig, L. M., Ohigashi, Y., Thurnauer, M. C., and Tiede, D. M (1998) *Biochemistry 37,* 8278−8281) and proton uptake by Q_B^- (Paddock, M. L., Graige, M. S., Feher, G., and Okamura, M. Y. (1999) *Proc. Natl. Acad. Sci. U.S.A. 96,* 6183−6188). Detailed EPR spectroscopic characterization of these Cu^{2+}−RCs will provide a means to investigate the role of local protein environments in modulating electron and proton transfer.

The structurally characterized photosynthetic bacterial reaction center protein (RC) provides a useful native system to explore the nature of protein motion coupled to biological electron transfer. In the RC, electron transfer occurs sequentially following the photoexcitation of a special pair of bacteriochlorophylls (P). The primary radical pair P^+H^-, where H denotes a monomeric bacteriopheophytin, is formed within ∼3 ps of photoexcitation of P. Within ∼200 ps, the electron is transferred from H^- to the primary ubiquinone acceptor (Q_A), yielding the membrane-spanning secondary radical pair $P^+Q_A^-$. The electron reaches the final quinone acceptor Q_B within about 200 μs. After a two-electron, two-proton reduction, Q_BH_2 is released from the RC, transporting electrons and protons to other redox components in the bacteria. The electron transfer between Q_A and Q_B is temperature activated (*1*−*3*), coupled to proton movement (*4*, *5*), and believed to be rate-limited by protein motion (*6*−*8*). While it is widely accepted that protein conformational changes play an important part in biological electron transfer, there is little experimental information on the role of anisotropic local protein environments in modulating electron transfer.

Recently, we detected a local protein environment, a Zn site, that apparently controls protein dynamics important for electron transfer in the RC (*9*). Isolated RCs from *Rhodobacter sphaeroides* R-26 were found to bind Zn^{2+} stoichiometrically and in a site distinct from the non-heme high spin Fe^{2+} site, which is buried in the protein interior between Q_A and Q_B. When Zn^{2+} is bound to this site, electron transfer between the quinones Q_A and Q_B ($Q_A^-Q_B \rightarrow Q_AQ_B^-$) is slowed and the room-temperature kinetics become distributed across the microsecond to millisecond time domain. Remarkably, the localized Zn^{2+} binding event mimics the global temperature effect of cooling the RCs (no Zn^{2+}) to 2 °C. We proposed that Zn^{2+} binding alters the dynamics of conformational changes in the RC, thereby influencing electron transfer (*9*). This work has been extended to show that Zn^{2+} and Cd^{2+} binding influences the proton uptake of Q_B (*10*). Another electron-transfer step in the bacterial RC can be influenced by metal ions. A dramatic decrease in the electron-transfer rate from the H^- to Q_A occurs upon removal of the non-heme Fe^{2+} (*11*−*14*) due to a change in reorganization energy for this step (*15*). Likewise, metal ions have been shown to inhibit electron transport in Photosystem II (*16*−*20*). Clearly, metal binding can affect primary photo-

* Corresponding author: Lisa M. Utschig, Chemistry Division D-200, Argonne National Laboratory, 9700 S. Cass Ave., Argonne, IL 60439. Telephone: (630) 252-3544. Fax: (630) 252-9289. E-mail: utschig@anl.gov.

10.1021/bi991800t CCC: $19.00
Published on Web 02/26/2000

chemistry and provides an important probe for understanding the involvement of local protein environments in electron transfer. Herein, we have extended our studies of metal binding to include Cu^{2+}.

A knowledge of the nature and geometry of the ligands at the metal center is important for understanding the mechanism of metal ion-induced modulation of electron and proton transfer. Electron paramagnetic resonance (EPR) is a powerful technique for studying metal ions in metalloproteins, providing information that is complementary to the three-dimensional crystal structure of proteins as determined by X-rays. For example, EPR spectroscopy not only provides structural information about the directly bound metal ligands for a noncrystalline sample but also can provide information about electronic coupling with remote amino acids and magnetic interactions (exchange and dipole−dipole) between the metal center and other paramagnetic radical species in the protein. Cu^{2+} ion ($3d^9$) has proved to be a useful spin probe of protein metal sites by substitution of Cu^{2+} for the native metal ion (Fe^{2+}, Zn^{2+}) (*21*, *22*). We have used this method to interrogate the electronic structure of the RC metal sites (Fe site and Zn/surface site) and surrounding protein.

Previously, the structure of the Fe site had been investigated using continuous wave electron paramagnetic resonance (EPR) spectroscopy of Cu^{2+}-substituted RCs (*23*−*26*). Unlike the Zn site, which is in a more remote position from the quinones than the Fe site, the substitution of different divalent metal ions into the Fe site does not significantly alter $Q_A^-Q_B \rightarrow Q_AQ_B^-$ electron transfer (*27*). The Cu^{2+} was incorporated into the Fe site either biosynthetically (*24*) or biochemically (*23*, *25*). Interestingly, the EPR spectra observed were dependent on the preparation method and indicated different Cu^{2+} ligand geometries. Another report examined light-induced structural changes in Cu−RCs (*26*). Because these previous experiments were carried out prior to the observation that there is more than one RC metal binding site, we have repeated and revised the Fe-removal/Cu-substitution preparation methods. Reproducible procedures for the preparation of Cu−RCs, with Cu^{2+} specifically bound at the Fe site or the surface site, have been developed and these samples have been studied using continuous wave (cw) and pulsed EPR spectroscopy.

We have used electron spin−echo envelope modulation (ESEEM) spectroscopy to characterize the magnetic interactions between Cu^{2+} and weakly coupled magnetic nuclei in the RC. ESEEM spectroscopy is a particularly useful method for probing Cu^{2+} imidazole interactions in Cu-containing metalloproteins (*28*−*30*). With this technique, one observes periodicities (modulations) in the ESEEM envelope that arise from the interaction of the unpaired electron spin of Cu^{2+} with the nuclear spins of the so-called remote nitrogens of the Cu^{2+} ligating histidines, i.e., those imidazole nitrogens that are not coordinated to Cu^{2+} (*31*). In this paper, we present our initial characterization of Cu−RCs by ESEEM spectroscopy. These represent the first reported ESEEM spectra of Cu−RCs. Comparison of the ESEEM spectra obtained confirm that the Cu^{2+} surface site has a different geometry and is spatially distinct from the Cu^{2+} bound to the Fe site. Modulations were observed that are characteristic of remote imidazole nitrogen−Cu interactions, thus implicating histidine amino acid side chains as ligands to Cu^{2+} when bound to the surface site. We believe that surface bound Cu^{2+} is bound at or near the Zn site that modulates $Q_A^-Q_B \rightarrow Q_AQ_B^-$ electron transfer (*9*) and proton uptake by reduced Q_B (*10*). These results are consistent with the proposed location of the surface metal ion site, supporting the idea that Cu^{2+} is binding to two or more of the histidine ligands (H68, H126, H128, and L211) located beneath the Q_B binding pocket (*9*, *10*). Further delineation of the coordination environment of these specifically prepared Cu−RCs will aid in the spectroscopic resolution of the mechanism of metal ion-induced allosteric modulation of $Q_A^-Q_B \rightarrow Q_AQ_B^-$ electron transfer(*9*) and proton uptake by reduced Q_B (*10*).

EXPERIMENTAL PROCEDURES

Preparation of Fe-Removed/Cu-Substituted RCs: Binding Cu^{2+} to the Fe Site. Cu^{2+} was substituted into the Fe site using a modification to the procedure of Utschig (1997) for the preparation of Fe-removed/Zn-replaced RCs. Purified RCs (1.0 mL $OD_{803} = 25\ cm^{-1}$ in 10 mM Tris-HCl, pH 7.9, 10 μM EDTA, 280 mM NaCl, and 0.045% LDAO) were incubated 5 min at 25 °C in 2.4 mM *o*-phenanthroline, 9 mM Tris-HCl, and 0.18 mM ubiquinone-10. The stock solutions were 135 mM *o*-phenanthroline (30% ethanol), 1 M solution of Tris-HCl, pH 8.0. Ubiquinone-10 (Sigma) was added from a 2 mM stock solution prepared by suspending the quinone in 1% LDAO and heating to 65 °C. A 1.0 M sample of LiSCN was added to the RC solution from a 3.8 M LiSCN stock solution (concentration determined by ICP-AES) followed by ice temperature incubation. After 30 min, 1.5 mM $CuSO_4$ was added and the protein was again incubated on ice. After 30 min, the protein was transferred to 10 mm wide 12−14 000 MWCO dialysis tubing (Spectra/Por) and dialyzed 24−36 h at 4 °C vs 10 mM Tris-HCl, pH 7.9, 0.01 mM EDTA, 0.045% LDAO, and 5 g Chelex 100 metal-chelating resin (Bio-Rad). Precipitated Cu and Fe thiocyanate complexes (light green and pink precipitate) were spun down and removed. The Cu−RC samples were incubated with 280 mM NaCl for 30 min, followed by rapid freezing in liquid N_2. The samples were then thawed and concentrated with centricon-30 devices. Without the high salt, freeze−thaw step, the RCs would not consistently concentrate, forming films on the filter membrane. The final concentrated protein samples (~200 μM RC) were frozen in liquid N_2 and stored at −80 °C until used for EPR or metal analysis.

Preparation of Fe-containing Cu−RCs: Binding Cu^{2+} to the Surface Site. The carotenoidless mutant *Rb. sphaeroides* R-26 was grown under illumination on Mn-depleted Hutner's medium, since we have observed >50% incorporation of Mn into the Fe site when grown with 6×10^{-6} M $MnSO_4$ and 2.5×10^{-5} M $FeSO_4$ in the medium (*14*). Reaction centers from this photosynthetic bacterium were isolated according to the procedure of Tiede (*3*) adapted by Utschig (*14*). EDTA was present in all buffers throughout the preparation at a concentration of 10 μM. For the final step of the purification procedure, RCs were eluted from the DEAE-Sephacel column with 10 mM Tris-HCl at pH 7.9, 10 μM EDTA, 280 mM NaCl, and 0.045% lauryldimethyl-amine *N*-oxide (LDAO), or 0.8% octyl-β-glucoside (OG) as the detergent. Final 280/802 nm ratios were 1.2−1.3. Protein concentrations were determined with the extinction coefficient $\epsilon_{802} = 288\ mM^{-1}cm^{-1}$ (*32*).

Stoichiometric Cu^{2+} binding to the RC was not observed using the Tris-HCl based gel filtration methods detailed for Zn^{2+} binding (*9*). Less stringent dialysis methods were used to determine optimal buffer conditions for reproducible Cu^{2+} binding. The extent of Cu^{2+} binding varied with the type of buffer and detergent, concentration of NaCl, and amount of Cu^{2+} added. Nonspecific Cu^{2+} binding (2−3 mol equiv Cu per RC) was often observed initially when not enough competitor (NaCl) or excess Cu^{2+} (>400 μM) was added to the RC solution. One repeatable dialysis preparation of stoichiometric Cu−RCs involved incubation of the RC protein ($OD_{800} \sim 20$ cm^{-1}) with 400 μM $CuSO_4$ (50 mM stock solution) at ice temperature for 12 h. The incubation buffer contained 20 mM HEPES at pH 7.75, 10 mM NaCl, and 0.8% OG. The RCs were dialyzed for a total of 96 h, with 3 changes of the incubation buffer. The samples were concentrated to ∼200−250 μM ($OD_{800} \sim 60$−70 cm^{-1}) with microcon-50 filtration devices, frozen in liquid N_2, and stored at −80 °C until used for metal or EPR analysis.

Once Cu^{2+} binding conditions were established by dialysis, a protocol for gel filtration chromatography was determined. Typically, the RC protein ($OD_{800} \sim 10$ cm^{-1}) was incubated with ∼10 mol equiv of $CuSO_4$ at ice temperature for 12 h. The incubation buffer contained 10 mM HEPES at pH 7.9, 10−20 mM NaCl, and 0.8% OG. The free Cu^{2+} was separated from bound metal ion by gel filtration chromatography through a Sephadex G-25 (Pharmacia) column equilibrated with 10 mM HEPES at pH 7.9, 50 mM NaCl, and 0.8% OG. Alternatively, the detergent 0.045% LDAO can be used in place of OG. Cu^{2+} reproducibly binds stoichiometrically in the presence LDAO after incubation with 4−10 equiv of $CuSO_4$ in the presence of 20−50 mM NaCl.

To investigate the reversibility of Cu^{2+}-binding, Cu−RCs prepared by dialysis or gel filtration were dialyzed vs Chelex 100 for 48 h at 4 °C. Approximately 2 g of Chelex 100 per 100 mL of buffer containing 20 mM Tris-HCl at pH 7.9, 50 mM NaCl, 1 mM EDTA, and 0.8% OG were used. The pH of the buffer was adjusted after addition and equilibration with the Chelex 100 resin.

Metal Analysis. Inductively coupled plasma-atomic emission spectroscopy (ICP-AES) on a Thermo Jarell Ash Atomscan Advantage spectrometer was used to determine the amount of Fe, Mn, and Cu bound to the RC. ICP-AES enables rapid sequential multielement determination with minimal sample volume. The ICP-AES instrument is equipped with an axial plasma configuration. This setup provides greater detection limits than those obtained with the standard radial plasma. The analytical standard deviation for these measurements was ∼0.01. The metal content of the RCs was analyzed before and after addition of Cu^{2+}.

EPR Spectroscopy. Continuous wave EPR spectra were obtained to observe the first derivative Cu^{2+} signals and to observe the signals of $P_{865}{}^{+}[Fe^{2+}Q_A]^{-}$ or $P_{865}{}^{+}[Cu^{2+}Q_A]^{-}$ formed under continuous illumination. The X-band data were collected using a Bruker ESP300E EPR spectrometer with a Bruker X-band ER046XK-T bridge. Spectra were measured at 12 K. Light-induced signals were obtained by illumination with a Xenon lamp.

Pulsed EPR experiments were performed on a home-built homodyne pulsed X-band EPR spectrometer having quadrature detection with two independent pulse forming units in the excitation channels. The spectrometer is designed to perform the following experiments: echo-detected field swept EPR experiments, echo-decay and free-induction decay experiments, delay after laser flash (DAF) experiments, and two-dimensional (2D) experiments. For the DAF experiments, the system is coupled with an optical parametric oscillator (Opotek) pumped by a Nd:YAG laser (Quantel).

A schematic diagram of the microwave bridge is shown in Figure 1. The microwave excitation channel consists of two independent microwave pulse forming units (MPFU). MPFUs are used to create pulses having different phases and amplitudes within one pulse train. Following the MPFU, the pulses are amplified by the TWT (up to 1 kW) and directed through a high-power isolator and high-power attenuator to the microwave cavity. Different types of cavities may be used. In this particular experiment, a Bruker dielectric cavity (ER4118X-MD5) was employed.

The microwave signal from the cavity is directed through a circulator to the detection channel. An overall noise figure of the detection channel is 4 dB. The minimum separation between the first and the second pulses at which an echo signal is still observable (dead time) is 110 ns. This time is determined by the extra ringing after the microwave pulses from the TWT.

The entire system is controlled by a PC through a GPIB board. A pulsed programmer is used to control the pulse experiment. It produces triggers for the data acquisition system and laser and pulses for: PIN switches to create microwave pulses, TWT gate pulses, protection pulse for the low noise amplifier (LNA). The programmer consists of a function generator DS 345 and DG 535 pulse generators (both from Stanford Research), controlled by a PC. The number of pulse generators used is determined by the number of microwave pulses needed for an experiment. For an N-pulse experiment, N+1 DG 535 pulse generators are used. The software was written by Phillip Morse, Scientific Software Services. The data acquisition system consists of two SR 250 Boxcar Integrators (Stanford research), ADC-card 2210/2310 series (Real Time Devices), incorporated into a PC, and a 500 MHz LeCroy oscilloscope (5350A). The software is designed to acquire, accumulate, and save experimental data from two channels (quadrature detection). A fast transient response, as free-induction decay (FID) or line-shape of the echo signal, is acquired by the LeCroy oscilloscope.

The ESEEM experiments were performed at liquid helium temperature, using a three pulse ($\pi/2 - \tau - \pi/2 - T - \pi/2$) stimulated echo pulse sequence. Spectra were collected at different τ values ranging from 150 to 520 ns for each data set containing 500 points, at a magnetic field of 3350 G. Additional data sets were obtained by varying the magnetic field (2900 G, 3100G, and 3350G) at a τ of 180 ns. The repetition rate of the applied pulse sequence was 100 Hz, microwave frequency of 9.57 GHz, pulse width of 20−25 ns, and microwave pulse power of 16 dB.

RESULTS

LiSCN-based Fe-removal with Cu^{2+} Substitution. Stringent conditions of chaotropic treatment followed by time specific addition of Cu^{2+} are needed to remove the Fe^{2+} from and insert Cu^{2+} into the Fe site. As we detailed previously for

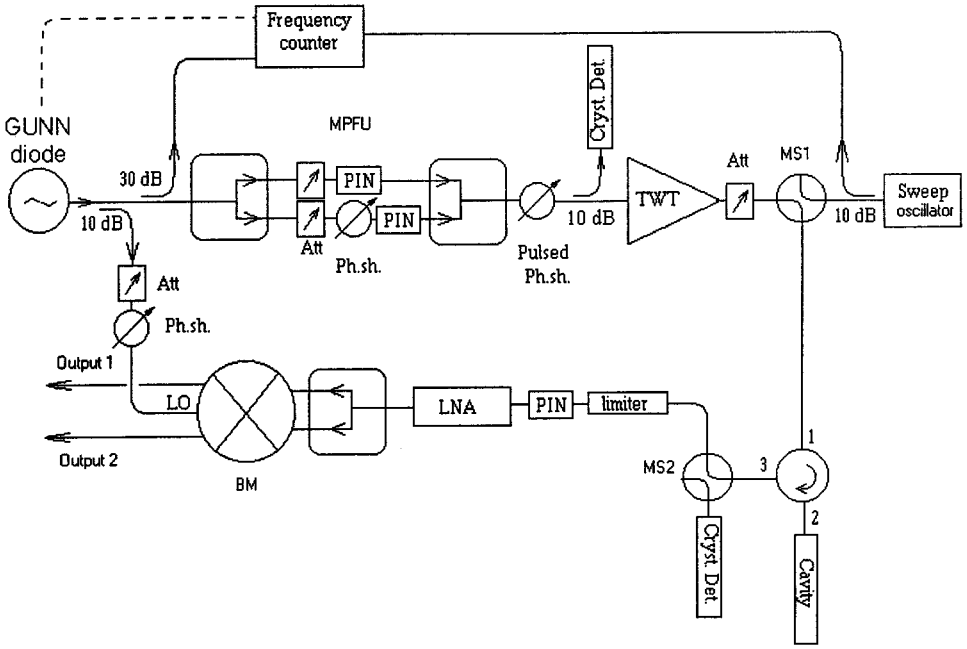

FIGURE 1: A schematic diagram of the microwave bridge for an X-band pulsed electron spin−echo spectrometer. The microwave source is a phase locked GUNN diode, which delivers ~200 mW in the frequency range of 8.3−9.57 GHz. Phase locking is arranged through a source locking microwave frequency counter (EIP 575) and shown as a dashed line. A 10 dB directional coupler after the GUNN is used for local oscillator (LO) of the quadrature balanced mixer (BM). The microwave excitation channel consists of two independent microwave pulse forming units (MPFU). In the first MPFU, there is an attenuator (Att). The second MPFU has an attenuator and a phase shifter (Ph. sh.) for phase adjustment. Microwave pulses are formed by PIN-diodes in the first and second channel. Pulses formed in the first MPFU and second MPFU are combined together and sent to the pulse phase shifter (Pulsed Ph.sh.) for the phase cycling and then to a pulsed microwave amplifier—Litton, model 624 Traveling Wave Tube (TWT). After amplification by the TWT, the pulses (up to 1 kW) are directed to the microwave cavity through a high-power isolator and high-power attenuator. There are two mechanical switches (MS): one in the excitation channel (MS1) and one in the detection channel (MS2). A crystal detector (Cryst. Det.) and microwave sweep oscillator (HP 8620C) are used for the tuning of the cavity and Q-factor measurement. In this particular experiment, a Bruker dielectric cavity (ER4118X-MD5) was employed. Typical widths of the $\pi/2$ pulses are 15−20 ns. The detection channel consists of a high-power limiter with a 1 dB insertion loss (Advanced Control Components), protection PIN-switch, low-noise amplifier (LNA, GaAs FET with 40 dB gain and 1.5 dB noise figure (JCA)), followed by DC filter, isolator, band-pass filter and balanced quadrature mixer (BM) from RHG. Two output 90° shifted signals from BM are fed to the video amplifier (DC-500 MHz) and then to boxcar integrators (SR 250) for computer acquisition. The bridge has several isolators, band-pass filters, and DC-blocks where required, which are not shown on the scheme.

Table 1: Metal/Protein Ratios Determined by ICP-AES Analysis of Various Preparations of *Rb. sphaeroides* RCs[a]

sample	Fe/RC	Cu/RC	preparation	no. of samples
purified R-26	1.0 ± 0.10	<0.03	Mn-depleted media	3
Cu_{sur}−RC	0.91 ± 0.15	1.0 ± 0.46[b]	Sephadex G25 column	7
Cu_{sur}−RC	0.85 ± 0.18	0.88 ± 0.20[b]	dialysis	4
Cu_{FeQ}−RC	0.35 ± 0.05	1.05 ± 0.55[c]	chaotropic treatment	4

[a] Standard deviations listed are for sample to sample variations resulting from differences between separate preparations. The actual analytical standard deviation for each individual measurement was less than 0.01. [b] Dialysis of the Cu−RCs against Chelex 100 resin reduces the Cu^{2+} content to <0.3 Cu/RC. [c] These samples were Chelex-treated prior to metal analysis.

our Fe-removal with Zn-replacement preparation (*9*), the successful incorporation of Cu^{2+} into the Fe site largely depends on the purification of the isolated RCs. The RC must be purified directly in 0.045% LDAO, and anion exchange chromatography performed such that the peak fractions collected have RC concentrations >80 μM. Several changes to the Zn-incorporation method were made. The amount of LiSCN was lowered from 1.5 to 1.0 M. This was done to achieve a delicate balance between having sufficient LiSCN present so that the Fe-thiocyanate complexes necessary for successful Fe-removal form and having a small enough amount of LiSCN present so that formation of similar Cu-thiocyanate complexes would not inhibit the incorporation of Cu^{2+} into the Fe site. Also, the concentration of *o*-phenanthroline was reduced. A high degree of nonspecific Cu-binding (Cu(I)-thiolates) was observed in the presence of 2-mercaptoethanol; therefore, this reagent was removed from the preparation solution. Only ~30−50% of the Cu−RCs retained the H-subunit. Even without the H-subunit, these Cu−RCs did not degrade (after 4 months at −80 °C) and had a deep blue color with a typical UV−vis spectrum for native RCs. Extensive treatment with Chelex 100 is necessary to remove adventitious Fe^{2+} and Cu^{2+}-thiocyanate complexes bound to the RC. Even after Chelex treatment, some Fe remains bound to the RC, as shown in Table 1. The remaining ~30% Fe is most likely residual surface-bound Fe based on EPR results, as previously reported (*14*).

It is important to add the Cu^{2+} during the chaotropic treatment with LiSCN in order to help retain the native structure. Previous methods for the preparation of Cu−RCs involved incubation of RCs with large quantities of Cu^{2+} several days after LiSCN-based Fe-removal (*6*, *25*, *27*). We

have attempted to bind metal ions to Fe-removed RCs (*14*) 24−48 h after chaotropic treatment. Metal-binding was observed only to RCs that were missing the H-subunit. In this case, the RCs appeared to readily bind excessive amounts of Cu^{2+} and were degraded (high A_{280}/A_{800} ratios), turning a blue-grey color with decreased absorbance and a blue shift in the 865 nm band. Extensive Chelex treatment was necessary to observe specific Cu-binding in these cases. Since it is possible that transition metal ions bind to other surface accessible site(s) in addition to/or instead of the Fe site, it is essential to determine the amount of Cu^{2+} incorporation via metal analysis after extensive Chelex treatment or by examination of the EPR spectral features.

Binding of Cu^{2+} to Fe-containing RCs. Stoichiometric Cu-binding (Cu/RC mole ratio of 1) can be obtained by incubating purified RCs with several equiv of $CuSO_4$, followed by gel filtration chromatography or extensive dialysis to remove unbound metal ion. Metal analysis of different experiments are tabulated in Table 1. Most samples were also analyzed for Fe and Mn content and found to contain ∼0.9 Fe and ∼0.1 Mn per RC. The content of Fe and Mn remained essentially unchanged from that determined for isolated RCs after the DEAE Sephacel column purification step, before Cu^{2+} addition. Thus, a total of 2 mol equiv of metal ion, 1 mol equiv each of Fe^{2+} and Cu^{2+}, are bound to the RC. These results indicate that Cu^{2+} does not displace Fe^{2+} and are similar to Zn^{2+} binding results previously reported (*9*). Unlike the previous observation with Zn^{2+}, a measurable amount of Cu^{2+} was not observed in purified RCs without addition of extra Cu^{2+} to the growth media.

Consistent Cu^{2+}-binding was achieved using HEPES buffer. Substoichiometric Cu-binding (Cu/RC mole ratio of 0.4) was always observed when Tris buffer was used. Tris apparently can form coordination complexes with divalent metal ions. This characteristic can be utilized as an advantage in some instances to reduce nonspecific metal ion binding to RCs. When the Cu-binding was done in HEPES, a "Good's" buffer that has a low-metal binding constant (*33*), metal analysis revealed more than one Cu bound (∼2−3 Cu per RC) if conditions were not stringent enough to reduce adventitious binding. The EPR spectra taken of these Cu−RCs (those with >1 Cu bound per RC) were weak and did not exhibit resolved Cu^{2+} hyperfine splittings.

Cu^{2+} bound to the RC by gel filtration or dialysis procedures detailed above can be removed by dialyzing Cu−RCs against the metal-chelating resin Chelex 100. Typically, dialyzing Cu−RCs (0.8−1.4 Cu/RC) vs Chelex 100 resin in a buffer containing Tris and EDTA for over 48 h reduces the Cu^{2+} content to ∼0.2−0.3 Cu/RC. In contrast, metal ions (Fe, Mn, Zn, or Cu) bound to the buried Fe site in native RCs are not removed by extensive Chelex treatment (Table 1) (*14*). Thus, the Chelex-accessibility exhibited by the Cu^{2+} is similar to that observed for Zn^{2+} (*9*). This result suggests that, like Zn^{2+}, a metal ion binding at the Cu^{2+}site is more easily exchanged, and hence, surface accessible. These results support the idea that the Zn^{2+} and Cu^{2+} are binding at a surface site on the RC. Furthermore, we have observed slowed $Q_A^-Q_B \rightarrow Q_AQ_B^-$ electron-transfer kinetics in the presence of $CuSO_4$ using transient optical techniques. Interestingly, the effect of Cu^{2+} differs from that of Zn^{2+} (*9*). Cu^{2+} apparently only influences the slow kinetic component of $Q_A^-Q_B \rightarrow Q_AQ_B^-$ electron transfer and also influences the P^+ recombination kinetics from Q_B. Elaboration of these results will be presented in a future paper (Utschig, L. M., and Tiede, D. M., unpublished results).

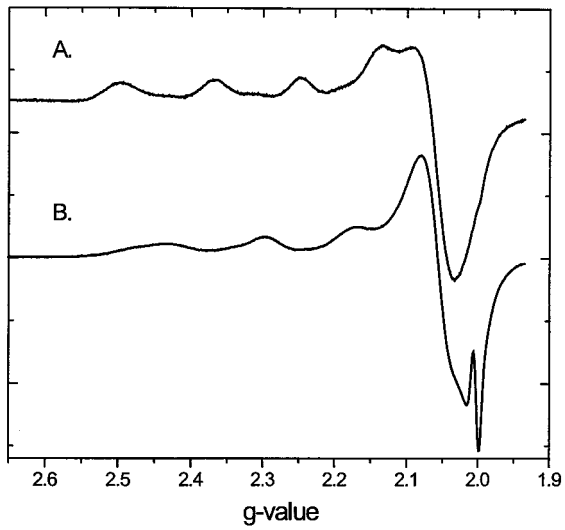

FIGURE 2: X-band EPR spectra of Cu−RCs, recorded in the dark at 12 K. (A) Spectrum of RCs with Cu^{2+} substituted into the Fe site following LiSCN chaotropic treatment as detailed in the text. The RCs were concentrated to $OD_{800} = 55\ cm^{-1}$ ($A_{280}/A_{800} = 1.4$) and had a final metal/protein ratio of 0.7 Cu/0.3 Fe/RC. (B) Spectrum of RCs (0.9 Cu/0.9 Fe/RC) with Cu^{2+} bound to the surface site of native Fe-containing RCs by dialysis methods and concentrated to $OD_{800} = 73\ cm^{-1}$ ($A_{280}/A_{800} = 1.2$). The data were collected at 9.14 GHz, with 20 G modulation amplitude, 2 mW microwave power, and 100 kHz modulation frequency.

CW EPR. We have used Cu^{2+} as a spin probe of the electronic structure of two RC metal sites and their local protein environments. The Cu^{2+} ion has a $3d^9$ electronic configuration with an effective spin $S = {}^1/_2$. All of our Cu−RC samples contain copper in natural isotopic abundance (^{63}Cu, 69.1%; ^{65}Cu, 30.1%). Both isotopes have nuclear spins with $I = 3/2$ and magnetic moments differing by 6.6%. Therefore, two magnetic isotopes contribute to each spectrum. Others have reported EPR data on RCs in which the Fe^{2+} was chemically replaced by Cu^{2+} (*23*, *25*, *27*). We revisited these experiments for two specific reasons: to validate our preparation methods of Fe-removed/Cu-substituted RCs and to provide a benchmark for comparison of the RCs with Cu^{2+} bound to the surface site.

The EPR spectrum of a frozen solution of RCs with Cu^{2+} substituted into the Fe site is shown in Figure 2A. Four peaks arising from the hyperfine coupling of the unpaired spin of Cu^{2+} with the nuclear spin of the Cu (^{65}Cu and ^{63}Cu) are observed at low magnetic field with $A_{||} = 143$ G. The g tensor is typical for Cu^{2+} in axial symmetry, corresponding to a $d(x^2 - y^2)$ ground-state orbital for the unpaired electron, with $g_{||} = 2.307$ and $g_{\perp} = 2.070$. The observed spectrum is comparable to that previously observed for Cu−RCs prepared by a similar method (*25*), suggesting that we have successfully incorporated Cu^{2+} into the Fe site with our new procedure. An underlying signal from $[Cu^{2+}Q_A]^-$ is observed (*25*). Thus, apparently a small amount of Q_A (∼12%) remains reduced after the Fe-removal/Cu-replacement procedure, even after dark adaptation of the sample.

By analogy with the X-ray structure of the Fe site (*34*−*36*), Cu^{2+} could be coordinated by four histidine residues (two each from the L and M subunits) and to one glutamic

acid acting as a bidentate ligand. From analysis of the superhyperfine interaction with ^{14}N and ^{15}N in ^{65}Cu-enriched samples, Calvo et al. concluded that only three histidine ligands are directly coordinated to the Cu^{2+} (*25*). The observed EPR spectrum for the chemically substituted Cu^{2+} *Rb. sphaeroides* R-26 via chaotropic LiSCN treatment differs from that reported by Buchanan and Dismukes (1987) for RCs from *Rb. sphaeroides* (strain Y) that had biosynthetically incorporated Cu^{2+} into the Fe site. EPR experiments of these RCs yielded different g values and copper hyperfine parameters from those of R-26, showing well-resolved hyperfine couplings with four nitrogen ligands. We found it difficult to isolate purified RCs with stoichiometric Cu^{2+} from wild-type *Rb. sphaeroides* cells grown in the presence of Cu^{2+}. The yields of RCs were very low, making purification and ICP-AES analysis difficult. In our relatively pure RCs ($A_{280}/A_{800} = 1.6$) we did not observe well-resolved $A_{||}$ and $A_{\perp}$ hyperfine couplings, even after extensive Chelex 100 treatment to remove adventitious Cu (~0.8 Cu/RC ratio after Chelex treatment).

The EPR spectrum of stoichiometric complexes of Cu^{2+} bound to native Fe-containing RCs via dialysis or gel filtration methods has different hyperfine coupling and g tensors than the spectrum of Cu^{2+} bound to the Fe site (Figure 2B). The EPR spectrum shows a hyperfine structure for the nuclear spin of Cu (^{65}Cu and ^{63}Cu) with $A_{||} = 160$ G. The g tensors $g_{||} = 2.238$ and $g_{\perp} = 2.057$ are nearly axially symmetric, consistent with tetragonal symmetry for the coordinated ligands (*21*, *22*, *37*). Resolved nitrogen hyperfine coupling in $g_{||}$ and $g_{\perp}$ was not observed (this coupling is not commonly observed in Cu proteins), a result of overlapping ^{65}Cu and ^{63}Cu resonances or a disordered metal site. The observed spectrum is typical of type 2 or "normal" copper EPR signals (*38*), having g and A values characteristic of most cupric complexes. Spectral simulations showed that an "extra" or "overshoot" peak (*22*) in the $g_{\perp}$ region ($g \sim 2.03$) results from line broadening due to orientational anisotropy of the hyperfine interaction. A residual dark signal from P^+ is observed at $g = 2.0026$.

Further evidence that there are two distinct Cu^{2+} sites on the RC was provided by the light-induced EPR spectra shown in Figure 3. The EPR spectrum of RCs with Cu^{2+} in the Fe site changes drastically upon illumination. The observed spectrum is similar to that observed when the quinone acceptor is reduced chemically $[Cu^{2+}Q_A]^-$ (*25*), originating from the exchange and dipole−dipole interactions between the Cu^{2+} and Q_A^- spins. In addition, triplet ^3P is observed at magnetic fields of ~3449 and 3059 G, which could arise from a small amount of residual $Cu^{2+}Q_A^-$ in the samples (present in the dark spectrum), or a slowed electron-transfer rate (k_Q) from the pheophytin to Q_A resulting from Fe-removal procedure (*11*−*15*). In contrast, the hyperfine features of the sample with Cu^{2+} bound to native Fe-containing RCs is essentially unchanged for the dark versus light-induced spectra. Thus, this Cu^{2+} is in a remote position removed from Q_A^- as well as P^+. An estimation of dipole−dipole coupling based on the observed line broadening (<2 G) suggests that this Cu^{2+} center lies >23 Å away from the light-induced radicals. Furthermore, these light-induced signals show that Cu^{2+} is binding specifically in each preparation as almost all or none of each signal changes upon irradiation. When illuminated at 4 K, native Fe-containing

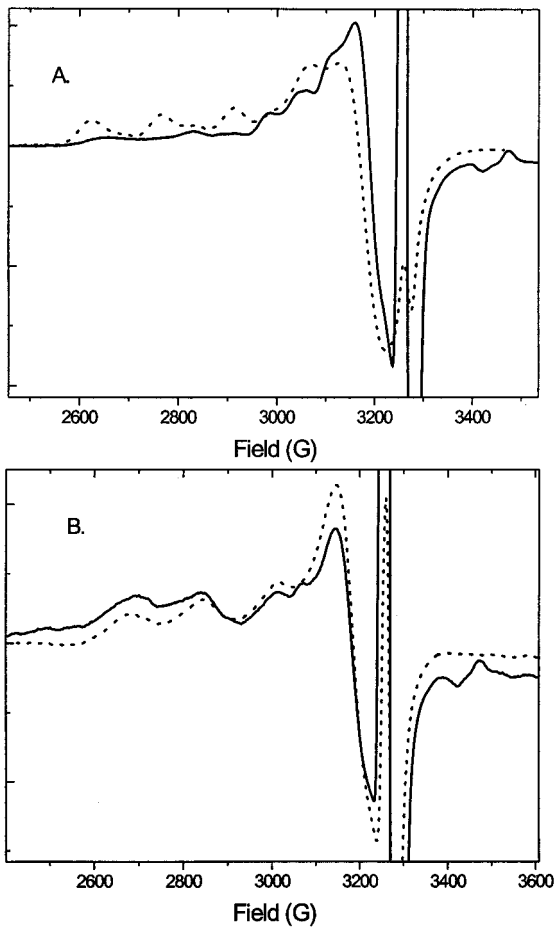

FIGURE 3: Light-induced X-band EPR spectra of Cu−RCs. Light-induced spectra (solid line) were measured at 12 K under continuous illumination with a Xenon lamp. The X-band data were collected for RCs with Cu^{2+} bound to the (A) Fe site and (B) surface site, as described in Figure 2. Dark spectra (dotted line) are displayed for comparison.

RCs from *Rb. sphaeroides* exhibit EPR signals from the radical pair $P^+[Fe^{2+}Q_A]^-$, with $g = 2.0026$ for P^+ and $[Fe^{2+}Q_A]^-$ exhibiting a broad resonance centered at ~1.8 (*39*, *40*). For Cu^{2+} bound to native Fe-containing RCs, an intense light-induced signal at $g = 2.0026$ was observed, corresponding to $P^+[Fe^{2+}Q_A]^-$. Likewise, a light-induced signal at $g = 2.0029$ is attributed to P^+ (with a small contribution from $[Cu^{2+}Q_A]^-$) for the Cu-substituted/Fe-removed samples.

ESEEM Spectroscopy. Pulsed EPR spectroscopy was used to examine the nature of the ligands at the Cu^{2+} site (*28*−*30*). Three-pulse ESEEM spectra of Cu-substituted RCs are presented in Figure 4. The magnetic field for the time-domain ESEEM data shown was set at the maximal three pulse echo-induced field swept (ESE) EPR intensity for the observed signal at $g = 2.07$ or $g = 2.06$. Figure 5 displays the Fourier transforms of the time-domain ESEEM data. The observed spectra resemble spectra observed for Cu^{2+}−imidazole model compounds (*31*, *41*−*43*) and for several Cu^{2+}−proteins. (*44*−*55*)

The spectra for RCs with Cu^{2+} in the Fe site exhibit two intense peaks at 0.42 and 1.53 MHz, with shoulders indicating several overlapping peaks. Such spectral features are characteristic of weakly hyperfine-coupled ^{14}N nuclei in close proximity to a paramagnetic species (Cu^{2+}) near the

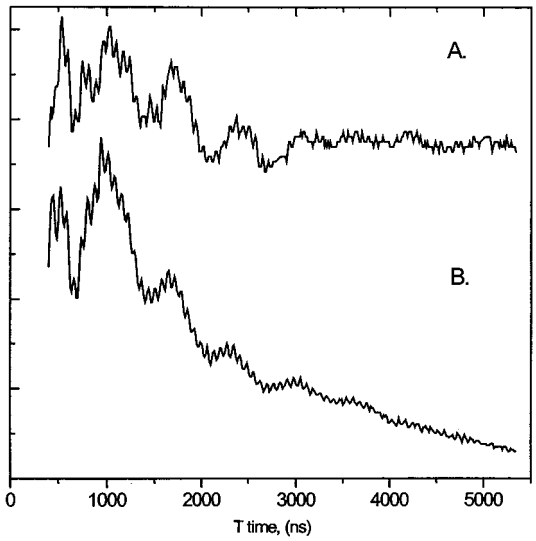

FIGURE 4: Three-pulse ESEEM spectra of Cu−RCs with (A) Cu^{2+} in the Fe site and (B) Cu^{2+} bound to the surface site. The time domain spectra are displayed. Experimental parameters: magnetic field 3335 G, microwave frequency 9.57 GHz, pulse width 20 ns, $\tau = 180$ ns, 100 Hz repetition rate. Temperature: (A) 7 K, (B) 4 K.

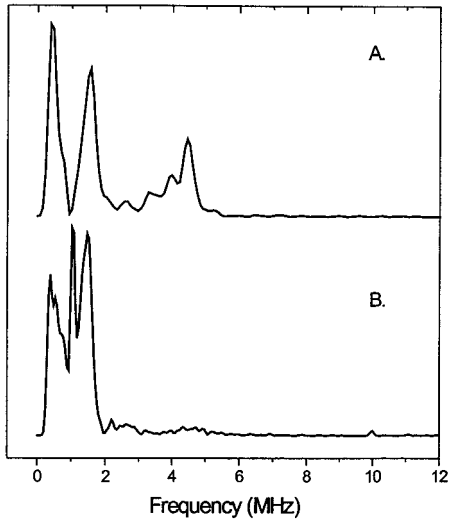

FIGURE 5: Fourier transforms of the three-pulse time domain ESEEM spectra shown in Figure 4.

"exact cancellation" limit (*31*, *56*). At this limit, in one of the electron spin manifolds, the splitting of the ^{14}N nuclear Zeeman interaction is canceled by that of the hyperfine interaction, typically giving rise to three low-frequency transitions below 2 MHz (*31*). These transition frequencies arise from the ^{14}N nuclear quadrupole interaction (nqi) and are invariant with applied magnetic field. Other features of the ESEEM spectrum include several shallow overlapping bands with peaks at 3.3, 4.0, and 4.4 MHz. These correspond to the so-called $\Delta M_I = 2$ transition, which exhibits a typical frequency of ~4 MHz (*28*). The remaining nqi feature observed in Figure 5A, the weak 2.6 MHz feature, can be assigned as a combination band (*45*, *49*, *51*). The presence of such a feature indicates multiple magnetically equivalent ^{14}N nuclei at the Cu^{2+} center, consistent with the Cu^{2+} binding to several histidine ligands. These ESEEM spectral results agree with previous CW EPR studies, which showed that the Cu^{2+} is ligated to three histidine ligands when incorporated into the Fe site using biochemical procedures (*25*).

The ESEEM spectrum of Cu^{2+} bound to the surface site is clearly different from the spectrum of Cu^{2+} in the Fe site, providing evidence that the Cu^{2+} is bound to a site distinct from the Fe site. We found that observation of the time-domain signal was more temperature-dependent than that from the sample with Cu^{2+} in the Fe site. This is consistent with the shorter relaxation time, which can be seen by comparing Figure 4B with 4A and indicates a fast relaxer, Fe^{2+}, coupled to the Cu^{2+}. At a magnetic field of the maximum ESE-detected EPR spectrum, narrow intense bands are observed at 0.42, 1.05, and 1.50 MHz, with shoulders at 0.56 and 0.75 MHz (Figure 5). These transition frequencies were invariant at different applied magnetic fields and result from ^{14}N nuclear quadrupole interactions (*31*, *56*). A very low intensity, broad peak is observed at ~4.5 MHz. This peak moved linearly with the magnetic field, indicating that it corresponds to the $\Delta M_I = 2$ transition (*28*). In addition, small combination peaks centered at ~2.5 MHz are observed, indicating more than one remote ^{14}N in the vicinity of the Cu^{2+} (*45*, *49*, *51*). The intensity of these combination peaks varied, depending on the value chosen for τ.

The nqi for the $I = 1$ ^{14}N nucleus is parametrized by the quadrupolar coupling constant e^2qQ, and the asymmetry parameter, η, and can be used to indicate the type of ^{14}N nuclei involved in the coupling. Both e^2qQ and η can be directly computed from the nqi frequencies using the relationships $\nu_{\pm} = 3/4\ e^2qQ\ (1 \pm \eta/3)$ and $\nu_o = {}^1/_2\ e^2qQ\ \eta$ (*30*, *54*). We assigned the frequencies as $\nu_o = 0.42$, $\nu_- = 1.05$, and $\nu_+ = 1.5$ and determined values of 0.5 for η and 1.68 for e^2qQ. These parameters are quite similar to those observed for other proteins that are known to exhibit copper coordination by histidines (*48*−*50*, *52*−*54*). Thus, modulations were observed that are characteristic of remote imidazole nitrogen−Cu interactions and most likely more than one histidine amino acid side chain is ligated to the Cu^{2+}. These results are consistent with the proposed location of the second metal ion site, supporting the idea that Cu^{2+} is binding to more than one of the histidine ligands (H68, H126, H128, and L211) located beneath the Q_B binding pocket (*9*). Future work will involve experiments to determine the number of coordinated histidines and the structure of the Cu^{2+} site.

DISCUSSION

Spectroscopic Evidence for Two Distinct and Geometrically Different Cu^{2+} Sites. The primary photochemistry of RC proteins can be influenced by metal ions. Hence, the examination of metal site structure and local protein environment are important for understanding the mechanism of metal ion-induced modulation of electron and proton transfer. Herein, we use paramagnetic Cu^{2+} to spectroscopically probe two metal sites on the RC: the well characterized Fe−quinone site and a second surface site, which we believe to be at or near the Zn site that regulates $Q_A^- Q_B \rightarrow Q_A Q_B^-$ electron transfer. We report refined procedures for the preparation of Fe-removed/Cu-substituted RCs with Cu^{2+} bound to the Fe site as well as reproducible methods for the stoichiometric binding of Cu^{2+} to a surface site on native, Fe-containing RCs.

The cw and pulsed EPR results clearly indicate two spectroscopically distinct Cu^{2+} sites for Cu−RCs prepared

by different methods. A cw EPR spectrum typical of a type 2 or normal copper center (*38*), with $A_{||}$ hyperfine of 160 G and axially symmetric *g*-tensors of $g_{||} = 2.24$, and $g_{\perp} = 2.06$, was observed for RCs with Cu^{2+} bound to the surface site. The relationship of the observed values on a $g_{||}$ vs $A_{||}$ plot (*21*, *22*) is consistent with a tetragonal type 2 Cu^{2+} environment. The $g_{||}$ and $A_{||}$ parameters fall between the two sets of values reported for Cu^{2+} in the Fe site. A tetragonal metal site, with little distortion away from a coplanar set of four nitrogen ligands, was proposed for biosynthetically incorporated Cu−RCs (strain Y) with values of $g_{||} = 2.19$, $A_{||} = 199$ G, and $g_{\perp} = 2.05$ (*24*). In contrast, the chaotropically treated Fe-removed RCs (strain R-26) substituted with Cu^{2+} RCs, described here and elsewhere (*23*, *25*), exhibited values of $g_{||} = 2.31$, $A_{||} = 143$ G, and $g_{\perp} = 2.07$ with hyperfine couplings to three nitrogen ligands, and has been interpreted as a distorted octahedral environment. Hence, the surface Cu^{2+} site has a different coordination environment than the Cu^{2+} coordination sphere of the Fe site.

In addition to the distinguishing cw EPR spectra, several other factors provide direct evidence that the Cu^{2+} is not binding to the Fe site when Cu^{2+} is bound to native RCs, using dialysis or size exclusion chromatography methods. The echo envelope decay time of the surface Cu^{2+} signal is fast relative to that of the signal observed when Cu^{2+} is in the Fe site. This is consistent with the presence of a nearby Fe^{2+}, corroborating the metal analysis that revealed a total of two mole equiv of metal ion, 1 mol equiv each of Cu^{2+} and Fe^{2+}, bound to the RC (Table 1). Furthermore, the Cu^{2+} EPR signal does not change in the light, indicating that this Cu^{2+} does not magnetically interact with light-induced radicals P^+ or Q_A^-. In contrast, the Cu^{2+} bound to the Fe site is magnetically coupled by exchange and dipole−dipole interactions with the unpaired spin of Q_A^- (*25*), as shown by the light-induced spectrum.

Location of the Surface-bound Cu^{2+}. The results from the ESEEM experiment provide spectroscopic evidence that the surface Cu^{2+} site on the RC contains two or more histidine ligands. The nuclear quadrupole interaction parameters for the $I = 1$ ^{14}N nucleus ($e^2qQ = 1.68$, $\eta = 0.5$) are comparable to those observed for other proteins with copper histidine ligation (*48*−*50*, *52*−*54*). Interestingly, the observed values are nearly identical to those reported for phenylalanine hydroxylase ($e^2qQ = 1.68$, $\eta = 0.55$) where two or more histidines bind to the Cu^{2+} center (*49*). *NQI* parameters in this range have been interpreted as arising either from the remote nitrogen of the coordinated histidine side chain residing in a hydrophobic environment or only weakly hydrogen bonded (*50*). Most likely candidates for the surface site histidine ligands include H68, H126, H128, and L211 (*9*). These histidines are positioned beneath the Q_B binding pocket and surround a water channel that is proposed to be a proton pathway to Q_B (*35*, *57*, *58*).

A second metal ion site was not observed in the original *Rb. sphaeroides* RC X-ray crystal structures (*34*−*36*), most likely because Zn^{2+} was not bound to the RCs under the crystallization conditions employed. Recent, preliminary X-ray diffraction results have been reported, which show that Zn^{2+} and Cd^{2+} in the surface metal site are ligated by His-H126, His-H128, and Asp-124 (*10*). Thus, our ESEEM results are consistent with the X-ray structural results and suggest that Cu^{2+} coordinates at or near the same site as the Zn^{2+} and Cd^{2+}. Estimates based on simulations of line broadening of the Cu^{2+} light-induced signal show that the Cu^{2+} is at least 23 Å removed from the radical Q_A^-. On the basis of the crystal structure, Q_A is a distance of ∼30 Å from His-H126. Furthermore, the similarity of both stoichiometric preparation and Chelex accessibility of Zn^{2+} (*9*) and Cu−RCs implicate comparable binding sites as does the slowed $Q_A^-Q_B \rightarrow Q_AQ_B^-$ electron-transfer kinetics observed in the presence of $CuSO_4$ (Utschig, L. M., and Tiede, D. M., unpublished results). For these reasons, we believe that the surface accessible Cu^{2+} is bound at or near the Zn site that modulates electron transfer between the quinones Q_A and Q_B ($Q_A^-Q_B \rightarrow Q_AQ_B^-$) (*9*) and proton uptake of Q_B^- (*10*).

Determining the role of the metal ion in regulating electron and proton transfer will require correlation of the metal site structure with electron- and proton-transfer events. Cu^{2+} provides a useful spectroscopic probe to concomitantly interrogate dynamic protein structure, metal site coordination environment (magnetic resonance techniques), and solution kinetics (transient optical measurements) for isolated and native membrane bound RCs. Binding of divalent metal ions to a specific coordination site on the RC potentially could alter the mobility of metal ligands and surrounding region of polypeptide as well as change essential electrostatic interactions important for electron and proton transfer. One proposal is that Zn^{2+} alters important localized protein motions of the RC that are necessary for rapid $Q_A^-Q_B \rightarrow Q_AQ_B^-$ electron transfer (*9*). Two alternative explanations for the mechanism of inhibition of proton transfer include that the metal ion is binding to ligands that act as proton donors, or that the metal ion electrostatically hinders proton uptake (*10*). Further delineation of the coordination environment of specifically prepared metal ion−RC complexes will help resolve the role of a localized metal ion site, i.e. electrostatic vs limiting protein dynamics, in influencing primary photochemistry events.

ACKNOWLEDGMENT

We thank S. Schlesselman, A. Wagner, T. Rajh, A. Smirnov, and P. Laible for technical assistance. This work was supported by the U. S. Department of Energy, Office of Basic Energy Sciences, Division of Chemical Sciences, under contract W-31-109-Eng-38.

REFERENCES

1. Li, J., Gilroy, D., Tiede, D. M., and Gunner, M. R. (1998) *Biochemistry 37*, 2818−2829.
2. Mancino, L., Dean, D., and Blankenship, R. (1984) *Biochim. Biophys. Acta 764*, 46−54.
3. Tiede, D. M., Vazquez, J., Cordova, J., and Marone, P. A. (1996) *Biochemistry 35*, 10763−10775.
4. Shinkarev, V. P., and Wraight, C. A. (1993) in *The Photosynthetic Reaction Center* (Deisenhofer, J., and Norris, J. R., Eds.) pp 193−255, Academic Press, Inc., San Diego.
5. Parson, W. W. (1987) in *Photosynthesis* (Amesz, J., Ed.) pp 43−61, Elsevier, New York.
6. Brzezincki, P., Okamura, M. Y., and Feher, G. (1992) in *The Photosynthetic Reaction Center II* (Breton, J., and Vermeglio, A., Eds.) pp 321−330, Plenum Press, New York.
7. Graige, M., Feher, G., and Okamura, M. (1996) *Biophys. J. 70*, SUAM4.
8. Graige, M. S., Feher, G., and Okamura, M. Y. (1998) *Proc. Natl. Acad. Sci. U.S.A. 95*, 11679−11684.

9. Utschig, L. M., Ohigashi, Y., Thurnauer, M. C., and Tiede, D. M. (1998) *Biochemistry 37*, 8278−8281.
10. Paddock, M. L., Graige, M. S., Feher, G., and Okamura, M. Y. (1999) *Proc. Natl. Acad. Sci. U.S.A. 96*, 6183−6188.
11. Blankenship, R. E., and Parson, W. W. (1979) *Biochim. Biophys. Acta 545*, 429−444.
12. Kirmaier, C., Holten, D., Debus, R. J., Feher, G., and Okamura, M. Y. (1986) *Proc. Natl. Acad. Sci. U.S.A. 83*, 6407−6411.
13. Liu, B., van Kan, P. J. M., and Hoff, A. J. (1991) *FEBS Lett. 289*, 23−28.
14. Utschig, L. M., Greenfield, S. R., Tang, J., Laible, P. D., and Thurnauer, M. C. (1997) *Biochemistry 36*, 8548−8558.
15. Tang, J., Utschig, L. M., Poluektov, O., and Thurnauer, M. C. (1999) *J. Phys. Chem. 103*, 5145−5150.
16. Yruela, I., Alfonso, M., Ortiz de Zarate, I., Montoya, G., and Picorel, R. (1993) *J. Biol. Chem. 268*, 1684−1689.
17. Schröder, W. P., Arellano, J. B., Bittner, T., Barón, M., Eckert, H., and Renger, G. (1994) *J. Biol. Chem. 269*, 32865−32870.
18. Barón, M., Arellano, J. B., and López-Gorgé, J. (1995) *Physiol. Plant. 94*, 174−180.
19. Jegerschöld, C., Arellano, J. B., Schröder, W. P., van Kan, P. J. M., Barón, M., and Styring, S. (1995) *Biochemistry 35*, 12747−12758.
20. Yruela, I., Gatzen, G., Picorel, R., and Holzwarth, A. R. (1996) *Biochemistry 35*, 9469−9474.
21. Peisach, J., and Blumberg, W. E. (1974) *Arch. Biochem. Biophys. 165*, 691−708.
22. Vänngård, T. (1972) in *Biological Applications of Spin Resonance* (Swartz, H. M., Bolton, J. R., and Borg, D. C., Eds.) pp 411−447, Wiley-Interscience, New York.
23. Feher, G., Isaacson, R. A., Debus, R. J., and Okamura, M. Y. (1986) *Biophys. J. 49*, 585a.
24. Buchanan, S. K., and Dismukes, G. C. (1987) *Biochemistry 26*, 5049−5055.
25. Calvo, R., Passeggi, M. C. G., Isaacson, R. A., Okamura, M. Y., and Feher, G. (1990) *Biophys. J. 58*, 149−165.
26. Smirnova, I. A., Blomberg, A., Andréasson, L.-E., and Brzezinski, P. (1998) *Photosynth. Res. 56*, 45−55.
27. Debus, R. J., Feher, G., and Okamura, M. Y. (1986) *Biochemistry 25*, 2276−2287.
28. Mims, W. B., and Peisach, J. (1979) in *Biological Applications of Magnetic Resonance* (Shulman, R. G., Ed.) pp 221−270, Academic Press, New York.
29. Mims, W. B., and Peisach, J. (1981) in *Biological Magnetic Resonance* (Berliner, L. J., and Reuben, J., Eds.) pp 213−263, Plenum, New York.
30. Peisach, J. (1993) in *Bioinorganic Chemistry of Copper* (Karlin, K. D., and Tyeklar, Z., Eds.) pp 21−33, Chapman & Hall, New York.
31. Mims, W. B., and Peisach, J. (1978) *J. Chem. Phys. 69*, 4921−4930.
32. Straley, S. C., Parson, W. W., Mauzerall, D. C., and Clayton, R. K. (1973) *Biochim. Biophys. Acta 305*, 597−609.
33. Blanchard, J. S. (1984) *Methods Enzymol. 104*, 404−414.
34. El-Kabbani, O., Chang, C.-H., Tiede, D. M., Norris, J., and Schiffer, M. (1991) *Biochemistry 30*, 5361−5369.
35. Ermler, U., Fritzsch, G., Buchanan, S., and Michel, H. (1994) *Structure 2*, 925−936.
36. Allen, J. P., Feher, G., Yeates, T. O., Komiya, H., and Rees, D. C. (1988) *Proc. Natl. Acad. Sci. U.S.A. 85*, 8487−8491.
37. Hathaway, B. J., and Billing, D. E. (1970) *Coord. Chem. Rev. 5*, 143.
38. Solomon, E. I., Penfield, K. W., and Wilcox, D. E. (1983) in *Structure and Bonding* pp 3−57, Springer-Verlag, Berlin.
39. Feher, G. (1971) *Photochem. Photobiol. 14*, 373−387.
40. Loach, P. A., and Hall, R. L. (1972) *Proc. Natl. Acad. Sci. U.S.A. 69*, 786−790.
41. Colaneri, M., and Peisach, J. (1992) *J. Am. Chem. Soc. 114*, 5335−5341.
42. Colaneri, M. J., and Peisach, J. (1995) *J. Am. Chem. Soc. 117*, 6308−6315.
43. Place, C., Zimmermann, J.-L., Mulliez, E., Guillot, G., Bois, C., and Chottard, J.-C. (1998) *Inorg. Chem. 37*, 4030−4039.
44. Mims, W. B., and Peisach, J. (1976) *Biochemistry 15*, 3863−3869.
45. Kosman, D., Peisach, J., and Mims, W. B. (1980) *Biochemistry 19*, 1304−1308.
46. Avigliano, L., Davis, J. L., Graziani, M. T., Marchesini, A., Mims, W. B., Mondovi, B., and Peisach, J. (1981) *FEBS Lett. 136*, 80−84.
47. Mondovi, B., Morpurgo, L., Agostinelli, E., Befani, O., McCracken, J., and Peisach, J. (1987) *Eur. J. Biochem. 168*, 503−507.
48. McCracken, J., Desai, P. R., Papdopoulos, N. J., Villafranca, J. J., and Peisach, J. (1988) *Biochemistry 27*, 4133−4137.
49. McCracken, J., Pember, S., Benkovic, S. J., Villafranca, J. J., Miller, R. J., and Peisach, J. (1988) *J. Am. Chem. Soc. 110*, 1069−1074.
50. Jiang, F., McCracken, J., and Peisach, J. (1990) *J. Am. Chem. Soc. 112*, 9035−9044.
51. Lu, J., Bender, C. J., McCracken, J., Peisach, J., Sevens, J. C., and McMillin, D. R. (1992) *Biochemistry 31*, 6265−6275.
52. Gurbiel, R. J., Peoples, R., Doan, P. E., Cline, J. F., McCracken, J., Peisach, J., Hoffman, B. M., and Valentine, J. S. (1993) *Inorg. Chem. 32*, 1813−1819.
53. Bubacco, L., Magliozzo, R. S., Wirt, M. D., Beltramini, M., Salvato, B., and Peisach, J. (1995) *Biochemistry 34*, 1524−1533.
54. Elliott, S. J., Randall, D. W., Britt, R. D., and Chan, S. I. (1998) *J. Am. Chem. Soc. 120*, 3247−3248.
55. van Gastel, M., Coremans, J. W. A., Jeuken, L. J. C., Canters, G. W., and Groenen, E. J. J. (1998) *J. Phys. Chem. A. 102*, 4462−4470.
56. Flanagan, H. L., and Singel, D. J. (1987) *J. Chem. Phys. 87*, 5606−5616.
57. Stowell, M. H. B., McPhillips, T. M., Rees, D. C., Soltis, S. M., Abresch, E., and Feher, G. (1997) *Science 276*, 812−816.
58. Ermler, U., Fitzsch, G., Buchanan, S., and Michel, H. (1992) in *Research in Photosynthesis* (Murata, N., Ed.) pp 341−347, Kluwer, Amsterdam.

BI991800T